

Machine-learning-optimized perovskite nanoplatelet synthesis

Carola Lampe¹ Ioannis Kouroudis² Milan Harth²

Stefan Martin¹ Alessio Gagliardi² Alexander S. Urban¹

¹ Nanospectroscopy Group and Center for NanoScience,
Nano-Institute Munich, Faculty of Physics

² Department of Electrical and Computer Engineering, Technical
University of Munich

Abstract

With the demand for renewable energy and efficient devices rapidly increasing, a need arises to find and optimize novel (nano)materials. This can be an extremely tedious process, often relying significantly on trial and error. Machine learning has emerged recently as a powerful alternative; however, most approaches require a substantial amount of data points, i.e., syntheses. Here, we merge three machine-learning models with Bayesian Optimization and are able to dramatically improve the quality of CsPbBr₃ nanoplatelets (NPLs) using only approximately 200 total syntheses. The algorithm can predict the resulting PL emission maxima of the NPL dispersions based on the precursor ratios, which lead to previously unobtainable 7 and 8 ML NPLs. Aided by heuristic knowledge, the algorithm should be easily applicable to other nanocrystal syntheses and significantly help to identify interesting compositions and rapidly improve their quality.

1 Introduction

Halide perovskite nanocrystals (PNCs), first demonstrated in 2014, have been rapidly improved, yielding tunability throughout the visible spectrum, quantum

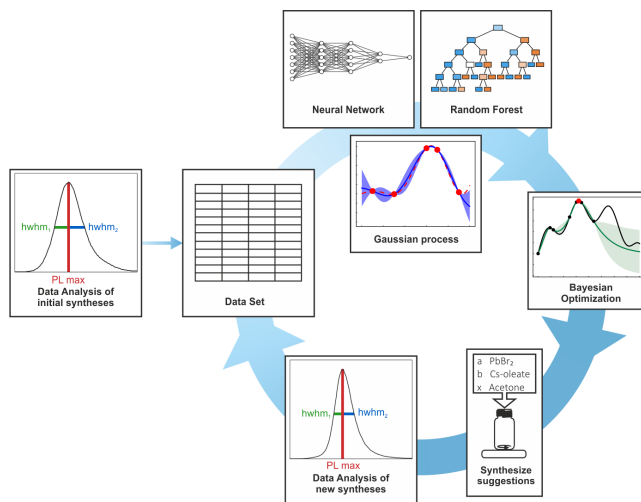


Figure 1: Scheme of the optimization process: Initially existing data points (syntheses) were analyzed and used to predict a spectral figure of merit (FoM) based on the narrowness and symmetry of their PL spectra using Gaussian Processes in combination with a Random Forest and a Neural Network. Constrained Bayesian optimization subsequently leverages the information of the artificial intelligence step to provide suggestions for new compositions. For each cycle, 14 new syntheses were carried out and characterized. The amended dataset is subjected to a new optimization cycle.

yields approaching 100%, and diverse geometries and sizes. Schmidt et al. [2014] Due to their exceptional properties, PNCs have already been incorporated into diverse applications, focusing on optoelectronics such as LEDs, solar cells, and photodetectors, but also in field-effect transistors and, even more recently, photocatalysis. Shamsi et al. [2019a], Abiram et al. [2022], Zhang et al. [2017], Gao et al. [2017], Shyamal et al. [2020] Despite these impressive improvements, several issues impede widespread commercialization, such as stability, lead toxicity, and spectral efficiency in the blue region of the visible spectrum. Schoonman [2015], Schileo and Grancini [2021], Weng et al. [2022] This latter effect is due to the chloride-perovskites being far from defect tolerant, resulting in extremely poor efficiencies compared to bromide- and iodide-based perovskites. Ye et al. [2021] Another way to tune the spectral response in PNCs is through quantum confinement. Especially, 2D nanoplatelets (NPLs) are ideal in this regard, as they exhibit no inhomogeneous broadening in the confined dimension, with only incremental thickness values possible - currently between 2 and 6 monolayers (MLs). Bohn et al. [2018] Analogous to the bulk-like Ruddlesden-Popper perovskites Stoumpos et al. [2016], their strong confinement can enable directional emission, boosting maximum external quantum efficiencies to 28%. Morgenstern et al. [2020] The quality of these colloidal quantum wells has improved signifi-

cantly; however, the quantum yields are still far from unity, and reproducibility is an issue. Improving the NPL quality or that of any NC dispersion is an arduous task, involving a vast possible number of parameters relating to composition and fabrication. Synthesizing all of these is both infeasible and unnecessary, as it is possible to create robust and data-efficient predictors to describe the outcome of changes in fabrication parameters. Mayr et al. [2022] Artificial neural networks (ANNs) have been widely used to approximate the quantities of interest, Chen and Pao [2019], Regonia et al. [2020] but success has also been achieved with, e.g., random forests and support vector machines. Baum et al. [2020], Rickert et al. [2021] It seems clear that no algorithm is universally superior, but rather each may be more suited for specific applications. Wolpert and Macready [1997] Despite their impressive results, these methods occasionally suffer from extrapolation into areas of input space with sparse or no data. Therefore, material science is a fertile ground for applying methods with inbuilt uncertainty quantification functionalities, such as Gaussian processes (GPs), which are especially attractive given their data efficiency and robustness against overfitting. Li et al. [2020], Zhang and Xu [2020], Seko and Ishiwata [2020] These methods provide an excellent set of predictors to determine the effect that different fabrication and chemical parameters have on the resulting material properties. Nevertheless, the optimal values of these parameters are not trivially determined. This field has lately been dominated by Bayesian optimization. In this scheme, the value of the predicted objective function is weighted against the intrinsic uncertainty of the prediction to balance the exploration of new areas against the exploitation of already acquired information. Balachandran et al. [2018], Voznyy et al. [2019]. However, this has required a massive experimental effort to achieve impressive results. In the future, models to optimize novel materials must focus on two aspects: incorporating multiple properties to increase the versatility of the targeted materials and reducing the number of syntheses necessary to achieve good results.

In this study, we develop a model addressing both of these issues as illustrated in Figure 1. By combining Gaussian processing with a neural network and a random forest classifier, we can significantly reduce the demand for optimizing the synthesis of 2D CsPbBr₃-based NPLs. The algorithm uses three precursor amounts to predict the emission wavelength of the resulting NPLs and the quality, i.e., the homogeneity of the photoluminescence (PL) spectra. Starting from a pool of 100 initial syntheses, we carried out seven rounds of optimization. The algorithm produced 14 new precursor combinations, which were then used for synthesis and the PL of the resulting dispersions measured. For all previously synthesized NPL thicknesses (2-6 ML), we significantly reduced the width and asymmetry of the PL emission, signifying higher homogeneity. Additionally, the algorithm effectively predicted precursor combinations leading to hitherto unobtained, thicker NPLs (7 and 8 MLs). The algorithm's performance was exceptional, especially considering the small amount of necessary experimental synthesizing.

2 Results and Discussion

In contrast to typical inorganic semiconductor NC syntheses and halide perovskite quantum dots, which rely on the hot-injection method, our synthesis is based on the ligand-assisted reprecipitation (LARP) method. Shamsi et al. [2019b, 2017], Bohn et al. [2018] Importantly, it is conducted at room temperature in ambient atmospheres. Bohn et al. [2018], Sichert et al. [2015], Tong et al. [2016] Briefly, a cesium-oleate precursor is injected into a PbBr_2 -ligand (comprising oleylamine and oleic acid) solution. After approximately 10 s, acetone, which acts as an antisolvent, is injected into the solution to induce NPL formation. After 60 s of vigorous stirring, the reaction is terminated by centrifugation at 1800 g for 3 min. The supernatant is discarded, and the precipitate is redispersed in hexane. Our previous studies determined that nanoplatelets (NPLs) form when the amount of the A-site cation, in this case, cesium, is restricted. Sichert et al. [2015] By fine-tuning the volumes of the cesium and lead-precursors and the anti-solvent, acetone, we were able to obtain nearly homogeneous dispersions of NPLs from 2 to 6 monolayers (MLs). Bohn et al. [2018] Accordingly, we chose these three parameters as the input parameters for the learning algorithm while keeping all others, e.g., synthesis time, temperature, and humidity, essentially constant. To quantify the quality of the synthesis, we acquired and analyzed PL spectra of the resulting dispersions. We chose not to focus on the PL intensity but rather on the narrowness and the spectral position of the PL emission. Accordingly, we determined the narrowness by the usual half width at half maximum (hwhm) metric, Kumar Reddy and Sagar [2015] while the symmetry was given by interpreting the spectrum as a distribution and calculating its skewness. Doane and Seward [2011]. As these two metrics have different ranges, they were normalized separately with the min-max method between 0 and 1 and subsequently added. This quantity is then normalized, yielding the figure of merit (FoM) of the respective synthesis:

$$FoM = \text{norm}\left[\frac{1}{f_{\text{sym}} + f_{\text{nar}}}\right]. \quad (1)$$

Accordingly, small values of f_{sym} and f_{nar} indicate good samples with a resulting FoM of 1 being a perfect spectrum and 0 a very poor one. Examples of poor spectra are shown in Figure 2a,b, and the best spectrum according to the metric obtained in Figure 2c. The goal of the machine-learning powered process is thus the maximization of the FoM. Several aspects must be considered when developing the full framework for guiding the NPL synthesis. Starting from a limited number of syntheses (100), we have to be sure to prevent overfitting. Therefore, to predict which precursor ratios yield the highest FoM values, we adopted a Gaussian process (GP) predictor using the python package scikit-learn. Pedregosa et al. [2011]. This choice was made because Gaussian Processes are generally more robust than others with a limited number of data. Our goal was to obtain ideal spectra for a given NPL thickness; hence, we needed a way to determine how many MLs the resulting NPLs would have. Due to the strong confinement of the NPLs, there is a robust correlation between thickness and

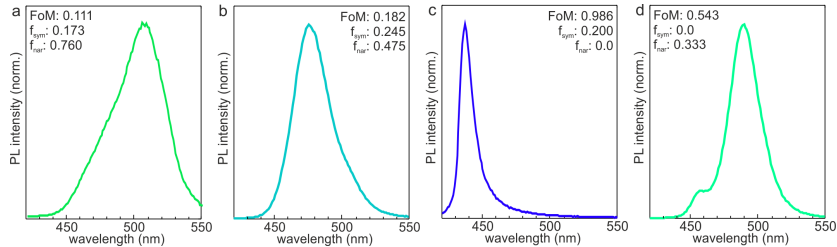


Figure 2: Examples of synthesized spectra with classification of their merit according to narrowness (f_{nar}), symmetry (f_{sym}) and overall quality (FoM). (a,b) Examples of poor spectra with (a) being extremely broad and (b) being quite asymmetric. (c) PL spectrum from the synthesis with the highest obtained FoM value. An extremely narrow spectrum compensates for the slight asymmetry. (d) The FoM calculation classifies this PL spectrum as very good due to a near-perfect symmetry. However, the short wavelength shoulder is a clear indicator of multiple thicknesses. This feature is predicted and preempted with the Random forest classifier.

PL emission wavelength. Bohn et al. [2018] We implemented a neural network through the tensorflow library Abadi et al. [2015] to predict the PL peak position based on the precursor ratios, starting from the pool of initial syntheses. We incorporated this into the overall FoM optimization pipeline as soft or hard Lagrange multipliers, constraining the PL to a given spectral window (see Table 1). In the soft case, we only incentivize and do not fully constrain PL emission near the mean of the spectral range. In contrast, in the hard case, the peak position is forced to fall on the mean, under the rationale that the suggestions will be least affected by the peak position prediction error. The hard constraints gave the best results in the initial stages of the optimization, when the peak position was still inaccurate, with the soft constraints giving better flexibility and therefore results when the peak position could be more accurately predicted. More details are given in the supporting information.

Table 1: NPL thickness and constraints for upper and lower limits

NPL thickness [ML]	2	3	4	5	6	7	8
lower limit [nm]	427	455	472	484	491	499	504
upper limit [nm]	438	467	479	489	498	503	507

In some syntheses, the PL spectrum revealed secondary peaks, which were not identified through the hwhm method, yet signify polydispersity, see Figure 2d. For this synthesis, the FoM is relatively high at 0.543; however, the shoulder at 455nm is a clear sign of an inhomogeneous NPL population. To increase the data efficiency of the optimization pipeline, we trained a random forest classifier with the aid of the library scikit-learn to identify the conditions

leading to polydisperse NPL distributions (see methods section for details). Importantly, while the classifier could identify roughly half of the combinations resulting in multiple peaks, it only erroneously excluded less than 5% of the combinations yielding single peaks (see SI for more details). Consequently, viable compositions are hardly prevented from being evaluated while large areas of compositional space are cordoned off, significantly improving the algorithm’s efficiency. The final set of considerations results from heuristic laboratory rules garnered from experience. Among these are minimum precursor volumes, the condition that the concentration of the Cs-precursor must be larger than the lead precursor to ensure NPL formation, and that the acetone volume is at least 30% of the total precursor volume to ensure the function as an antisolvent.

These individual contributions were merged into a Bayesian Optimization Framework to deliver suggestions for promising precursor ratios for new syntheses. This approach generates suggestions focusing initially on points with high uncertainty and gradually shifting toward known areas with a high payoff. The advantage of this method is that it exploits known space and explores potentially promising points, but it completely neglects areas with a low payoff and low uncertainty. This results in a very data-efficient scheme, as only a fraction of the parameter space is explored to reveal local maxima and minima. The tradeoff between exploitation and exploration is merged into a surrogate function which is then optimized. Not many data points are initially available, so the algorithm favors exploration at the cost of exploitation. However, over time, this balance shifts with further exploitation leading to a faster optimization of the surrogate function. In this phase, already acquired data points are exploited to refine suggestions and obtain optimized peaks. In this work, we used the Expected Improvement acquisition function to define the balance between exploration and exploitation (see Section 4.2 for details).

Specifically, we generated 100.000 random three-dimensional vectors (representing the precursor ratios), adhering to the heuristic constraints as mentioned earlier. For each NPL thickness, we determined the vectors with the highest overall optimization goal not predicted to exhibit a double peak, and synthesized NPLs with these precursor settings. Overall, we ran seven cycles with 14 syntheses per cycle for a total of 220 syntheses, including the initial ones. An overview of all the syntheses is given in Figure 3a,

where the syntheses are located in the three-dimensional input parameter space with the color signifying the emission wavelength. The overall trend is similar, with smaller Cs:Pb ratios leading to shorter emission wavelengths emanating from thinner NPLs. Note that the point density deviates significantly throughout the parameter space. This constitutes a visual representation of the algorithm initially exploring wide areas loosely and focusing on specific areas of high interest once it has developed a good understanding of the space. The quality of the PL spectra improved noticeably, as can be seen in SI for the case of 5 ML NPLs. The fwhm narrows considerably from 38 to 19 nm (193 to 99 meV), while the f_{sym} is reduced by 1.607 to 0, achieving perfect symmetry. Ad-

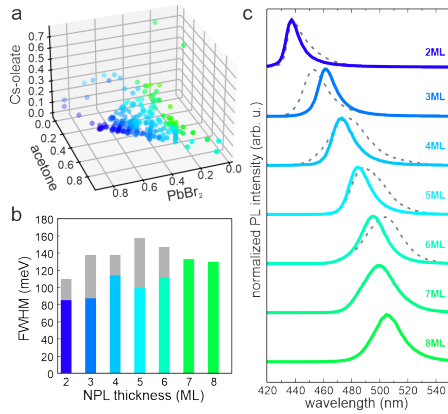


Figure 3: (a) Results of all synthesized NPL dispersions displayed in the three-dimensional precursor parameter space. The points are colored according to their respective PL emission maximum. (b) The narrowness of NPL spectra was measured by fwhm values (in meV) before optimization (gray bars) and after optimization (colored bars). A clear improvement is observed for all samples. (c) Optimized PL spectra for all NPL thicknesses (colored lines) compared to initial, typical PL spectra (dashed gray). As the 7 and 8 ML NPLs were only obtained through optimization, there are no initial spectra.

ditionally, the spectral position of the PL maximum shifts gradually from 490 nm to 486 nm. In terms of the FoM, this corresponds to an improvement from 0.429 to 0.916. Similar improvement was achieved for all previously established NPL thicknesses, as shown in Figure 3b, where the fwhm before (gray bars) and after optimization (colored) are shown for all thicknesses. The optimized spectra are displayed as colored curves in Figure 3c, where the dashed gray ones are from typical initial syntheses. All optimized spectra are significantly narrower and less asymmetric. All peak maxima exhibited a blueshift with the sole exception of the 3 ML NPLs. The improvement can also be seen in the FoM values, which increased substantially for all thicknesses. These are displayed in SI along with the precursor amounts (both new and old). While there are only subtle shifts in the precursor amounts for some thicknesses, there are also significant deviations, such as for the 4 ML and 6 ML NPLs. This demonstrates the advantage of the employed approach, as it is unlikely these precursor ratios would have been heuristically selected. The quality of the spectra is noticeable even when compared to the best spectra obtained from the initial NPL synthesis (see SI).Bohn et al. [2018]

The algorithm performed exceptionally well, as shown in Figure 4. With every new synthesis added to the training sets, the error in predicting the quality factor decreased substantially (Figure 4a). As the downward trend is still steep at the end of the implemented training data, the algorithm would prob-

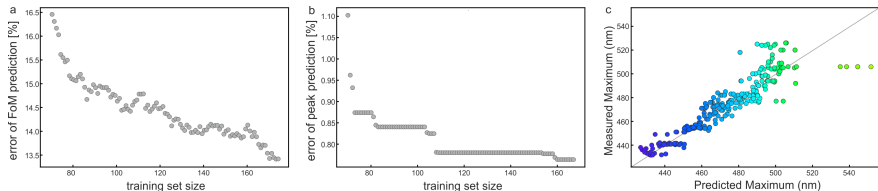


Figure 4: (a) Evolution of error for the FoM prediction with an increasing number of training samples. The error would likely decrease even further with additional syntheses. (b) Evolution of error for the peak position predictor with an increasing number of training samples. The initially low error has almost reached a plateau, confirming the high efficiency of the algorithm in predicting the resulting PL emission maxima. (c) The final accuracy of the peak position predictor. The outlier points correspond to rare occurrences in the dataset and hardly decrease the overall evaluation. All results were generated with a 90-10 training validation split and 10-fold validation.

ably improve further with more syntheses. In contrast, the predictor for the resulting PL emission wavelength improved rapidly for the first 30-40 syntheses, continued by a slower improvement (Figure 4b). This shows how well the precursor amounts define the PL emission of the resulting NPLs and that the algorithm could adapt quickly. The difference between predicted and measured PL emission maxima is highlighted in Figure 4c. Here, there is a very strong grouping of the points along the diagonal (indicated as grey line), indicative of very high accuracy. Interestingly, the algorithm predicted several precursor combinations to result in spectra with emission maxima at wavelengths longer than 494 nm, which corresponds to 6 ML NPLs. While not all of these resulted in NPLs, we were able to obtain two separate dispersions with distinct emission maxima at 501 nm and 505 nm, which we could assign to 7 ML and 8 ML NPLs, respectively and confirm through TEM imaging (see SI). We must note that the 8 ML NPL dispersion also contains small amounts of slightly thicker NPLs.

Nevertheless, the algorithm enabled us to obtain specific NPL thicknesses for the first time, which also helped determine important excitonic properties of the strongly confined asymmetric nanocrystals. Gramlich et al. [2022]. This is very impressive considering a) the significantly low amount of data (*i.e.* syntheses) being fed into the algorithm and b) the fact that no data points in this spectral region were provided, proving the strong extrapolative abilities of our pipeline. We carried out only 220 syntheses, which is more than an order of magnitude less than in similar studies. Voznyy et al. [2019] Our previous experience with the synthesis certainly helped streamline the process. Accordingly, in the next step, we will apply the algorithm to a novel synthesis, which we have not yet had experience with, and test how well it performs in this case and which parts might need further optimization. Also, to further increase turnaround time and enhance reproducibility, we will look into merging the algorithm with high throughput, automated synthesis via microfluidics with temperature control. Sun

et al. [2019], Lignos et al. [2020]

3 Conclusion

In summary, we have implemented a novel machine-learning method to obtain CsPbBr₃ NPLs of a given thickness and with high optical quality with a vastly reduced amount of data. The algorithm, comprising three machine-learning models merged with Bayesian optimization, can optimize the spectra’ quality, thus the monodispersity of the samples and the desired emission wavelength, *i.e.* the thickness of the resulting NPLs. Additionally, predicting and taking into account the purity of the resulting spectrum and incorporating additional heuristic constraints helped decrease the data pressure, meaning that the algorithm was able to rapidly improve the quality of NPL dispersions while requiring only at most three optimization cycles per NLP. In total, only 220 samples were required to obtain these results. Moreover, the model was able to identify precursor ratios leading to hitherto unobtainable NPL thicknesses, proving that the models could learn correlations beyond the training set bounds. The model can easily be expanded to account for additional synthetic parameters, such as temperature and humidity, and optimize quantum yields or stability. The next steps will constitute testing the versatility of the algorithm by transferring it to an unknown synthesis and implementing a high throughput automated synthesis via microfluidics to speed up the process and ensure higher reliability.

4 Experimental Section

4.1 Synthesis

Materials: Cs₂CO₃ (cesium carbonate, 99%), PbBr₂ (lead(II)bromide, > 98%), oleic acid (technical grad 90%), oleylamine (technical grade 70%), acetone (for HPLC, > 99.9%), toluene (for HPLC, > 99.9%) and hexane (for HPLC, > 97.0%, GC) were purchased from Sigma Aldrich and used without further purification.

The PbBr₂ ligand solution and Cs-oleate were prepared according to Bohn et al. [2018]. The synthesis procedure remained the same for all used synthesis parameters. It is presented in the following:

The synthesis was carried out under an ambient atmosphere at room temperature. The synthesis ratios were multiplied by 3 to get reasonable volumes to work with in the laboratory. A reaction glass was loaded with PbBr₂-precursor solution and Cs-oleate was immediately added under vigorous stirring. After 10 s, acetone was added quickly, and the reaction mixture was stirred for 1 min. Afterward, the mixture was centrifuged at 4000 rpm for 3 min, and the precipitate was redispersed in hexane (2 ml). Immediately after synthesis, the samples were optically characterized with a commercial spectrometer (FLOUROMAX-Plus, HORIBA).

4.2 Algorithm details

For the Gaussian Processes predicting the FoM the kernel employed was the sum of a radial basis function (RBF) and a Matern covariance function whose parameters were optimized by maximizing the log-marginal-likelihood (LML).

The neural network predicting the peak position consisted of three hidden layers with five neurons each. The first was activated using the Exponential Linear Unit (ELU) and the subsequent two with the Rectified Linear Unit (ReLU). The output layer activation was ELU. The weight initialization was the He uniform variance scaling initializer, and the optimizer used in this case was Root Mean Squared Propagation (RMSDrop) with an exponentially decaying learning rate.

The random forest classifier was trained with the constraint that every leaf should contain at least ten samples, and the optimization criterion reflecting the purity of each leaf is the gini index.

The Bayesian optimization scheme used the expected improvement acquisition function, constrained suitably with the constraints described in Section 2.

Supporting Information

Supporting Information is available from the Wiley Online Library or from the author.

Acknowledgements

The writers acknowledge funding from the following sources:

This project was funded by: the European Research Council Horizon 2020 through the ERC Grant Agreement PINNACLE (759744), by the Deutsche Forschungsgemeinschaft (DFG) under Germany’s Excellence Strategy EXC 2089/1-390776260, by the Bavarian State Ministry of Science, Research and Arts through the grant “Solar Technologies go Hybrid (SolTech)”,

the Project ProperPhotoMile, supported under the umbrella of SOLAR-ERA.NET Cofund 2 by The Spanish Ministry of Science and Education and the AEI under the project PCI2020-112185 and CDTI project number IDI-20210171; the Federal Ministry for Economic Affairs and Energy on the basis of a decision by the German Bundestag project number FKZ 03EE1070B and FKZ 03EE1070A and the Israel Ministry of Energy with project number 220-11-031. SOLAR-ERA.NET is supported by the European Commission within the EU Framework Programme for Research and Innovation HORIZON 2020 (Cofund ERA-NET Action, N 786483),

and by the “EXC 2089: e-conversion” DFG-cluster of excellence [project number: 390776260, <https://www.e-conversion.de/>]. ”ARTEMIS” - TUM innovation network, Technical University of Munich funded through the German Excellence Initiative and the state of Bavaria.

References

- Luciana C Schmidt, Antonio Pertegás, Soranyel González-Carrero, Olga Malinkiewicz, Said Agouram, Guillermo Minguez Espallargas, Henk J Bolink, Raquel E Galian, and Julia Pérez-Prieto. Nontemplate synthesis of $\text{CH}_3\text{NH}_3\text{PbBr}_3$ perovskite nanoparticles. *Journal of the American Chemical Society*, 136(3):850–853, 2014.
- Javad Shamsi, Alexander S Urban, Muhammad Imran, Luca De Trizio, and Liberato Manna. Metal halide perovskite nanocrystals: synthesis, post-synthesis modifications, and their optical properties. *Chemical reviews*, 119(5):3296–3348, 2019a.
- Gnanasampanthan Abiram, Murugathas Thanihaichelvan, Punniamoorthy Ravirajan, and Dhayalan Velauthapillai. Review on perovskite semiconductor field-effect transistors and their applications. *Nanomaterials*, 12(14):2396, 2022.
- Jingru Zhang, Qian Wang, Xisheng Zhang, Jiexuan Jiang, Zhenfei Gao, Zhiwen Jin, and Shengzhong Frank Liu. High-performance transparent ultraviolet photodetectors based on inorganic perovskite CsPbCl_3 nanocrystals. *RSC advances*, 7(58):36722–36727, 2017.
- Ge Gao, Qiaoyue Xi, Hua Zhou, Yongxia Zhao, Cunqi Wu, Lidan Wang, Pengran Guo, and Jingwei Xu. Novel inorganic perovskite quantum dots for photocatalysis. *Nanoscale*, 9(33):12032–12038, 2017.
- Sanjib Shyamal, Sumit Kumar Dutta, Tisita Das, Suvodeep Sen, Sudip Chakraborty, and Narayan Pradhan. Facets and defects in perovskite nanocrystals for photocatalytic CO_2 reduction. *The journal of physical chemistry letters*, 11(9):3608–3614, 2020.
- J Schoonman. Organic–inorganic lead halide perovskite solar cell materials: a possible stability problem. *Chemical Physics Letters*, 619:193–195, 2015.
- Giorgio Schileo and Giulia Grancini. Lead or no lead? availability, toxicity, sustainability and environmental impact of lead-free perovskite solar cells. *Journal of Materials Chemistry C*, 9(1):67–76, 2021.
- Shuchen Weng, Guicheng Yu, Chao Zhou, Fang Lin, Yonglei Han, Hao Wang, Xiaoxi Huang, Xiaoyuan Liu, Hanlin Hu, Wei Liu, et al. Challenges and opportunities for the blue perovskite quantum dot light-emitting diodes. *Crytals*, 12(7):929, 2022.
- Junzhi Ye, Mahdi Malekshahi Byranvand, Clara Otero Martínez, Robert LZ Hoye, Michael Saliba, and Lakshminarayana Polavarapu. Defect passivation in lead-halide perovskite nanocrystals and thin films: toward efficient leds and solar cells. *Angewandte Chemie*, 133(40):21804–21828, 2021.

- Bernhard J. Bohn, Yu Tong, Moritz Gramlich, May Ling Lai, Markus Doblinger, Kun Wang, Robert L. Z. Hoyer, Peter Müller Buschbaum, Samuel D. Stranks, Alexander S. Urban, Lakshminarayana Polavarapu, and Jochen Feldmann. Boosting tunable blue luminescence of halide perovskite nanoplatelets through postsynthetic surface trap repair. *Nano Letters*, 18(8):5231–5238, 2018. doi: 10.1021/acs.nanolett.8b02190. URL <https://doi.org/10.1021/acs.nanolett.8b02190>. PMID: 29990435.
- Constantinos C Stoumpos, Duyen H Cao, Daniel J Clark, Joshua Young, James M Rondinelli, Joon I Jang, Joseph T Hupp, and Mercouri G Kanatzidis. Ruddlesden–popper hybrid lead iodide perovskite 2d homologous semiconductors. *Chemistry of Materials*, 28(8):2852–2867, 2016.
- Thomas Morgenstern, Carola Lampe, Tassilo Naujoks, Matthew Jurow, Yi Liu, Alexander S. Urban, and Wolfgang Brütting. Elucidating the performance limits of perovskite nanocrystal light emitting diodes. *Journal of Luminescence*, 220:116939, 2020. ISSN 0022-2313. doi: <https://doi.org/10.1016/j.jlum.2019.116939>. URL <https://www.sciencedirect.com/science/article/pii/S0022231319313742>.
- Felix Mayr, Milan Harth, Ioannis Kouroudis, Michael Rinderle, and Alessio Gagliardi. Machine learning and optoelectronic materials discovery: A growing synergy. *The Journal of Physical Chemistry Letters*, 13:1940–1951, 2022.
- Hsin-An Chen and Chun-Wei Pao. Fast and accurate artificial neural network potential model for mapbi3 perovskite materials. *ACS omega*, 4(6):10950–10959, 2019.
- Paul Rossener Regonia, Christian Mark Pelicano, Ryosuke Tani, Atsushi Ishizumi, Hisao Yanagi, and Kazushi Ikeda. Predicting the band gap of zn quantum dots via supervised machine learning models. *Optik*, 207:164469, 2020.
- Fabio Baum, Tatiane Pretto, Ariadne Koche, and Marcos Jose Leite Santos. Machine learning tools to predict hot injection syntheses outcomes for ii–vi and iv–vi quantum dots. *The Journal of Physical Chemistry C*, 124(44):24298–24305, 2020.
- Carolin A Rickert, Elif N Hayta, Daniel M Selle, Ioannis Kouroudis, Milan Harth, Alessio Gagliardi, and Oliver Lieleg. Machine learning approach to analyze the surface properties of biological materials. *ACS Biomaterials Science & Engineering*, 7(9):4614–4625, 2021.
- David H Wolpert and William G Macready. No free lunch theorems for optimization. *IEEE transactions on evolutionary computation*, 1(1):67–82, 1997.
- Zheng Li, Luke EK Achenie, and Hongliang Xin. An adaptive machine learning strategy for accelerating discovery of perovskite electrocatalysts. *ACS Catalysis*, 10(7):4377–4384, 2020.

- Yun Zhang and Xiaojie Xu. Machine learning lattice constants for cubic perovskite compounds. *ChemistrySelect*, 5(32):9999–10009, 2020.
- Atsuto Seko and Shintaro Ishiwata. Prediction of perovskite-related structures in ACuO_{3-x} (a=ca, sr, ba, sc, y, la) using density functional theory and bayesian optimization. *Physical Review B*, 101(13):134101, 2020.
- Prasanna V Balachandran, Benjamin Kowalski, Alp Sehirlioglu, and Turab Lookman. Experimental search for high-temperature ferroelectric perovskites guided by two-step machine learning. *Nature communications*, 9(1):1–9, 2018.
- Oleksandr Voznyy, Larissa Levina, James Z Fan, Mikhail Askerka, Ankit Jain, Min-Jae Choi, Olivier Ouellette, Petar Todorovic, Laxmi K Sagar, and Edward H Sargent. Machine learning accelerates discovery of optimal colloidal quantum dot synthesis. *ACS nano*, 13(10):11122–11128, 2019.
- Javad Shamsi, Alexander S. Urban, Muhammad Imran, Luca De Trizio, and Liberato Manna. Metal halide perovskite nanocrystals: Synthesis, post-synthesis modifications, and their optical properties. *Chemical Reviews*, 119(5):3296–3348, 2019b. doi: 10.1021/acs.chemrev.8b00644. URL <https://doi.org/10.1021/acs.chemrev.8b00644>. PMID: 30758194.
- Javad Shamsi, Prachi Rastogi, Vincenzo Caligiuri, Ahmed L Abdelhady, Davide Spirito, Liberato Manna, and Roman Krahne. Bright-emitting perovskite films by large-scale synthesis and photoinduced solid-state transformation of CsPbBr_3 nanoplatelets. *ACS Nano*, 11(10):10206–10213, 2017. doi: 10.1021/acsnano.7b04761.
- Jasmina A Sichert, Yu Tong, Niklas Mutz, Mathias Vollmer, Stefan Fischer, Karolina Z Milowska, Ramon García Cortadella, Bert Nickel, Carlos Cardenas-Daw, Jacek K Stolarczyk, et al. Quantum size effect in organometal halide perovskite nanoplatelets. *Nano letters*, 15(10):6521–6527, 2015.
- Yu Tong, Eva Bladt, Meltem F Aygüler, Aurora Manzi, Karolina Z Milowska, Verena A Hintermayr, Pablo Docampo, Sara Bals, Alexander S Urban, Lakshminarayana Polavarapu, et al. Highly luminescent cesium lead halide perovskite nanocrystals with tunable composition and thickness by ultrasonication. *Angewandte Chemie International Edition*, 55(44):13887–13892, 2016.
- Andra Naresh Kumar Reddy and Dasari Karuna Sagar. Half-width at half-maximum, full-width at half-maximum analysis for resolution of asymmetrically apodized optical systems with slit apertures. *Pramana*, 84(1):117–126, 2015.
- David P Doane and Lori E Seward. Measuring skewness: a forgotten statistic? *Journal of statistics education*, 19(2), 2011.
- F. Pedregosa, G. Varoquaux, A. Gramfort, V. Michel, B. Thirion, O. Grisel, M. Blondel, P. Prettenhofer, R. Weiss, V. Dubourg, J. Vanderplas, A. Passos,

- D. Cournapeau, M. Brucher, M. Perrot, and E. Duchesnay. Scikit-learn: Machine learning in Python. *Journal of Machine Learning Research*, 12: 2825–2830, 2011.
- Martín Abadi, Ashish Agarwal, Paul Barham, Eugene Brevdo, Zhifeng Chen, Craig Citro, Greg S. Corrado, Andy Davis, Jeffrey Dean, Matthieu Devin, Sanjay Ghemawat, Ian Goodfellow, Andrew Harp, Geoffrey Irving, Michael Isard, Yangqing Jia, Rafal Jozefowicz, Lukasz Kaiser, Manjunath Kudlur, Josh Levenberg, Dandelion Mané, Rajat Monga, Sherry Moore, Derek Murray, Chris Olah, Mike Schuster, Jonathon Shlens, Benoit Steiner, Ilya Sutskever, Kunal Talwar, Paul Tucker, Vincent Vanhoucke, Vijay Vasudevan, Fernanda Viégas, Oriol Vinyals, Pete Warden, Martin Wattenberg, Martin Wicke, Yuan Yu, and Xiaoqiang Zheng. TensorFlow: Large-scale machine learning on heterogeneous systems, 2015. URL <https://www.tensorflow.org/>. Software available from tensorflow.org.
- Moritz Gramlich, Michael W. Swift, Carola Lampe, John L. Lyons, Markus Döblinger, Alexander L. Efros, Peter C. Sercel, and Alexander S. Urban. Dark and bright excitons in halide perovskite nanoplatelets. *Advanced Science*, 9(5): 2103013, 2022. doi: <https://doi.org/10.1002/advs.202103013>. URL <https://onlinelibrary.wiley.com/doi/abs/10.1002/advs.202103013>.
- Shijing Sun, Noor TP Hartono, Zekun D Ren, Felipe Oviedo, Antonio M Buscemi, Mariya Layurova, De Xin Chen, Tofunmi Ogunfunmi, Janak Thapa, Savitha Ramasamy, et al. Accelerated development of perovskite-inspired materials via high-throughput synthesis and machine-learning diagnosis. *Joule*, 3(6):1437–1451, 2019.
- Ioannis Lignos, Richard M. Maceiczky, Maksym V. Kovalenko, and Stavros Stavarakis. Tracking the fluorescence lifetimes of cesium lead halide perovskite nanocrystals during their synthesis using a fully automated optofluidic platform. *Chemistry of Materials*, 32(1):27–37, 2020. doi: 10.1021/acs.chemmater.9b03438.